Spatial and energy distributions of X-ray emissions from leaders in natural and rocket triggered lightning

M. M. Schaal,[1] J. R. Dwyer,[1] Z. H. Saleh,[2] H. K. Rassoul,[1] J. D. Hill,[3] D. M. Jordan,[3] and M. A. Uman[3]

Received 4 April 2012; revised 13 June 2012; accepted 18 June 2012; published 2 August 2012.

[1] Energetic radiation is known to be produced by lightning. To investigate these emissions, ground-based observations are being conducted at the International Center for Lightning Research and Testing (ICLRT) at Camp Blanding, FL where measurements of energetic radiation from both natural and rocket-triggered lightning discharges are recorded. In the present study, data from two natural negative cloud-to-ground stepped leaders and one rocket-triggered "chaotic" dart leader are analyzed in detail to investigate X-ray energy spectra and spatial X-ray distributions around the source. These measurements are compared with Monte Carlo simulations of runaway electron propagation with the goal of understanding the underlying mechanism of runaway electron production and their role in lightning initiation and propagation. We show that the energetic electrons that produce X-rays exhibit a characteristic energy less than 3 MeV for two natural and one rocket-triggered leaders investigated. In addition to studying these three leaders, energetic electron luminosity, total energy, and energetic electron per meter are compared to the following return stroke currents for 28 leaders from 12 different triggered flashes. Electron luminosity is found to increase exponentially with return stroke current up to about 10 kA and to be roughly constant for larger currents. The maximum electron luminosity, which is determined indirectly through X-ray luminosities, is on the order of 10^{17} electrons/s, which is less than the value found from theoretical calculations.

Citation: Schaal, M. M., J. R. Dwyer, Z. H. Saleh, H. K. Rassoul, J. D. Hill, D. M. Jordan, and M. A. Uman (2012), Spatial and energy distributions of X-ray emissions from leaders in natural and rocket triggered lightning, *J. Geophys. Res.*, *117*, D15201, doi:10.1029/2012JD017897.

1. Introduction

[2] Despite decades of research, many mysteries remain about the properties of X-ray emission from lightning [*Dwyer et al.*, 2012]. Prior to 2001, evidence of X-ray emission from lightning was ambiguous due to inadequate measurements and the sporadic nature of natural lightning [*Suszcynsky et al.*, 1996]. While some earlier papers [*McCarthy and Parks*, 1985, 1992; *Eack et al.*, 1996a] showed credible evidence for X-ray emission in thunderstorms, the case for X-ray emission from lightning remained uncertain.

[3] Using aircraft, *McCarthy and Parks* [1985, 1992] measured ionizing radiation with energies from 5 to 110 keV inside thunderstorms. This flux of radiation was observed to increase prior to the discharge of lightning and was attributed to bremsstrahlung emission from energetic electrons. The number density of energetic electrons decreased at the time of the lightning discharge. The mechanism of the energetic electron emission could not be identified.

[4] *Eack et al.* [1996a, 1996b], using NaI detectors on sounding balloons, measured a flux of X-rays while the balloons were inside and above thunderclouds. The X-ray emission lasted longer than the typical duration of a lightning flash, so it was concluded that lightning was probably not the only cause for the X-ray emission. Instead, the X-ray flux was attributed to the large scale electric field inside the thunderstorm [*Wilson*, 1925; *McCarthy and Parks*, 1992].

[5] The first reliable detection of energetic radiation associated with lightning was made by *Moore et al.* [2001] who measured energetic emissions from three natural cloud-to-ground lightning strikes in coincidence with electric field changes. These bursts of radiation began 1 to 2 ms before the start of the return stroke and continued to just before the return stroke. *Moore et al.* [2001] could not distinguish the energetic emissions between X-rays and electrons. Furthermore, the spatial source of the emission could not be determined, although the stepped leader was inferred to be that source from the time of occurrence of the radiation.

[6] *Dwyer et al.* [2003] recorded energetic radiation during the dart-stepped leader phase of rocket-triggered lightning. They found that the dart-stepped leaders produced energetic

[1]Department of Physics and Space Sciences, Florida Institute of Technology, Melbourne, Florida, USA.
[2]Medical Physics Department, Memorial Sloan-Kettering Cancer Center, New York, New York, USA.
[3]Department of Electrical and Computer Engineering, University of Florida, Gainesville, Florida, USA.

Corresponding author: M. M. Schaal, Department of Physics and Space Sciences, Florida Institute of Technology, Melbourne, FL 32901, USA. (meagan.schaal@gmail.com).

0148-0227/12/2012JD017897

radiation up to 160 μs prior to the return strokes. By the use of attenuators, *Dwyer et al.* [2004] showed that almost all of the energetic radiation was composed of X-rays and that the emission extended to about 250 keV. Additionally, the bottom 50 m of the channel was found to be the source of most emission and the emission increased as the leader tip approached the ground. X-rays from rocket-triggered lightning dart-stepped leaders were found to arrive in discrete bursts, with each pulse lasting less than 1 μs.

[7] *Dwyer* [2004] compared triggered lightning X-ray observations with the Relativistic Runaway Electron Avalanche (RREA) model [*Gurevich et al.*, 1992; *Gurevich and Zybin*, 2001; *Dwyer et al.*, 2003] and found that RREA could not explain the low X-ray energy and high flux that was observed from dart leaders [*Dwyer et al.*, 2004]. Furthermore, *Dwyer* [2004] suggested that the Cold Runaway Electron Model was responsible for the dart leader X-ray emission. Unlike RREA, the Cold Runaway Electron Model does not result in a particular average runaway electron energy, but does require an electric field an order-of-magnitude larger than the conventional breakdown field, 3×10^6 V/m at sea level.

[8] *Dwyer et al.* [2005] reported X-ray bursts associated with stepped leaders in natural cloud-to-ground lightning. The X-ray emission was remarkably similar to the bursts from dart-stepped leaders, indicating a common production mechanism. *Dwyer et al.* [2005] also demonstrated that X-rays are usually emitted during the leader step formation and so are closely related to the stepping process.

[9] *Saleh et al.* [2009] further described the properties of X-ray emission from triggered lightning. Specifically, one triggered dart-stepped leader and two triggered dart leaders were analyzed to obtain a modeled X-ray energy spectrum, a luminosity evolution of electrons, and an empirical relation for the radial (around the source leader) X-ray distribution. *Saleh et al.* [2009] found that deposited energy measured at the ground falls off proportional to $e^{-r/120}/r$ where r is the cylindrical radial distance in meters from the lightning channel. They also concluded that the electron source of the emission is not beamed downward, but emitted isotropically with an average electron energy of about 1 MeV, which is consistent with *Hill et al.* [2012], who measured single photon energies up to 2 MeV for one "chaotic" dart leader (a leader with unusual dE/dt measurements) preceding a rocket-triggered lightning return stroke. Using Monte Carlo simulations, the average luminosity (average production rate) of energetic electrons was deduced to be $\sim 1 \times 10^{16}$ electrons/s for one dart-stepped leader and increased as the source approached the ground. The maximum X-ray luminosity was found to be 3.5×10^{15} s^{-1} with the total X-ray deposited energy at the ground being about 10^{12} MeV. *Saleh et al.* [2009] suggested that the energetic electron luminosity had implications for Terrestrial Gamma Ray Flashes (TGFs). Since TGFs are now thought to originate from within thunderclouds, a runaway electron source must also be present. *Saleh et al.* [2009] found that 2.7×10^{13} energetic seed electrons per TGF per leader was the appropriate value to model the observed flux of a TGF.

[10] Although many questions regarding X-ray emission have been clarified, the exact mechanism and source location of the X-ray production in lightning leaders has not been well-established [*Dwyer et al.*, 2005; *Howard et al.*, 2010; *Hill et al.*, 2012]. In this paper, following the approach of *Saleh et al.* [2009], we present new information about the properties of X-ray emission from natural and rocket-triggered lightning as observed by the Thunderstorm Energetic Radiation Array (TERA). Measured X-ray energy spectra will be presented for one natural stepped leader and one triggered "chaotic" dart leader as well as radial energy distributions, average electron and X-ray luminosities. We provide an updated model for investigating natural lightning, building on *Saleh et al.* [2009]. Additionally, electron luminosities, total energies, and energetic electron per meter and correlations between X-ray emission and return stroke peak currents are given for 28 lightning leaders.

2. Instrumentation

[11] TERA measures energetic radiation in the form of X-rays and gamma-rays (energies ranging from 30 keV to several MeV) from natural and rocket-triggered lightning. TERA is located at the International Center for Lightning Research and Testing (ICLRT) at the Camp Blanding Army National Guard Base in north-central Florida and is operated jointly by the University of Florida and Florida Institute of Technology. The facility covers an area of approximately 1 km^2 and has been measuring X-rays from lightning since 2002. In tandem with TERA, another experiment called the Multiple Station Experiment (MSE) measures the vertical component of electric fields and their derivatives using wideband flat plate antennas as well as the horizontal magnetic field using loop antennas. Together the TERA/MSE network is composed of 25 TERA instruments and over 20 (10 dE/dt, 10 E-field, 4 magnetic field, 2 optical) MSE sensors [*Hill et al.*, 2012]. The layout, as of September 2010, is shown in Figure 1. In addition, the source locations of the radiated electric field derivative signals and the X-ray signals were determined in three dimensions by the 10 station TERA/MSE network via a time-of-arrival (TOA) network. The TOA network is described in further detail in *Hill et al.* [2012].

[12] TERA is composed of 25 separate aluminum boxes designed specifically to exclude light, water, and RF noise [*Dwyer et al.*, 2003, 2004, 2005]. The 0.32 cm thick aluminum box becomes transparent at X-ray energies greater than about 30 keV. Each box houses either one or two NaI(Tl)/PMT (photomultiplier tube) detectors with the necessary fiber optics and electronics for control [*Dwyer*, 2009].

[13] The aluminum boxes are welded at every seam. The top of the box lifts off to access the equipment and detectors inside. The lid of the box is clamped down to the sides of the lower box, with gasket lining the edges to ensure a secure fit. The two detectors are inserted into PVC type tubes on opposite corners to secure them into place. One of the potential two detectors has the option to be placed in a lead attenuator that absorbs X-ray energies below about 300 keV. The lead attenuator extends 4.5 cm above the top of the PMT and 41 cm below the top to completely cover the PMT and its base. A lead cap at the top of the attenuator fits over the tube. Both the tube and the cap are 0.32 cm thick. Enclosing the detectors in lead provides a means of determining the X-ray energies by comparing the unshielded (unattenuated) detector to the shielded detector.

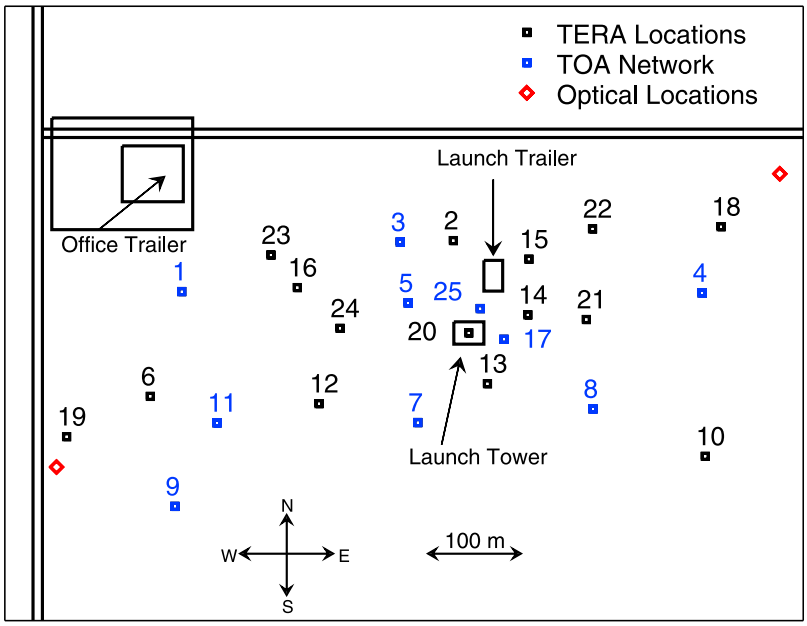

Figure 1. Overview of the ICLRT site for 2009–10 at Camp Blanding, FL. Station 20 is located at the top of the launch tower about 12 m above the ground. Stations marked in blue indicate the stations used for the dE/dt TOA network (but are also TERA locations). Optical measurement locations are marked in red.

[14] Each TERA box is operated remotely through a set of so-called PIC controllers that connect to the launch control trailer via 62.5 μm fiber optics. Within each box, Opticomm FM fiber optic transmitters are used to transmit the PMT anode signals to the data acquisition system located in a shielded launch control trailer powered by a generator. Fiber optic propagation delays have been measured and corrected for in the analysis. At launch control, each box can be powered on or off, and monitored for temperature or voltage fluctuations.

[15] TERA is comprised of 36 Sodium Iodide (NaI) and two Lanthanum Bromide ($LaBr_3$) detectors. Each NaI(Tl)/PMT and $LaBr_3$(Ce)/PMT detector contains a 7.62 cm $\times$ 7.62 cm cylindrical scintillator that is optically coupled to the photomultiplier tube. Each scintillator/PMT combination is then connected to a PMT base that produces a signal via the anode channel. These detectors display a fast light decay time of 16 ns as compared to the NaI detectors (250 ns). The $LaBr_3$ detectors also emit about 60% more light than the NaI detectors near 1 MeV photon energies.

[16] TERA receives its power through solar panels that are installed at each station. The solar panel charges a 12 V battery inside each box. When the system is armed, the PMTs are powered by the battery and protected by a fuse.

[17] The oscilloscopes recording the TERA instrument outputs are triggered by two optical sensors at opposite corners of the ICLRT for natural or triggered lightning or by incident current measuring at least 6 kA at the rocket launcher for triggered lightning [*Howard et al.*, 2010]. The current is measured directly below the launcher with a non-inductive T&M Research R-7000-10 current viewing resistor (CVR) with a bandwidth from DC to 8 MHz [*Hill et al.*, 2012]. Two, 16 channel, Yokogawa DL 716 Scopecorders and one, 16 channel, Yokogawa DL 750 Scopecorder in tandem record the signals from the 36 PMT anode channels via fiber optic cables. Two seconds of data with 1 second of pre-trigger sampling are recorded at a sampling rate of 10 million samples per second for one of the scopes, while the other two scopes record 0.8 seconds of pre-trigger sampling and 1.6 seconds of data. All three scopes are digitized with 12-bit amplitude resolution. One, 4 channel, Lecroy digital storage oscilloscope records data from the $LaBr_3$/PMTs at a sampling rate of 250 MHz with 2.5 ms of pre-trigger sampling. All of the other sensors, including the TOA network, are recorded in a similar fashion. Further details about TERA are described in *Saleh et al.* [2009].

3. TERA Observations

[18] The ICLRT measured and recorded 18 rocket-triggered lightning flashes and two natural strikes in 2009. Twelve successful rocket-triggered flashes that produced at least one return stroke and two natural lightning strikes were measured at the facility in 2010. The data for this report is from flashes MSE 10-01 on June 30, 2010, MSE 07-04 on July 16, 2007, and UF 10-20 on July 15, 2010 and is exclusively shown in all figures except for the last two, which include 28 leader events (including the flash UF 10-20) from 2009–10. MSE refers to a natural flash and is followed by the year, e.g., 07, and the flash number, e.g., 04. Similarly, UF refers to a rocket-triggered flash and is followed by the year and flash number. Of the 12 rocket-triggered flashes in 2010, continuous X-ray emissions (as a result of X-rays arriving at the detector quicker than the width of a single photon response pulse) from four "chaotic" dart leaders in triggered lightning were observed on all NaI and $LaBr_3$ detectors beginning on average about 10 μs prior to the onset of the return stroke [*Hill et al.*, 2012]. These dart leaders

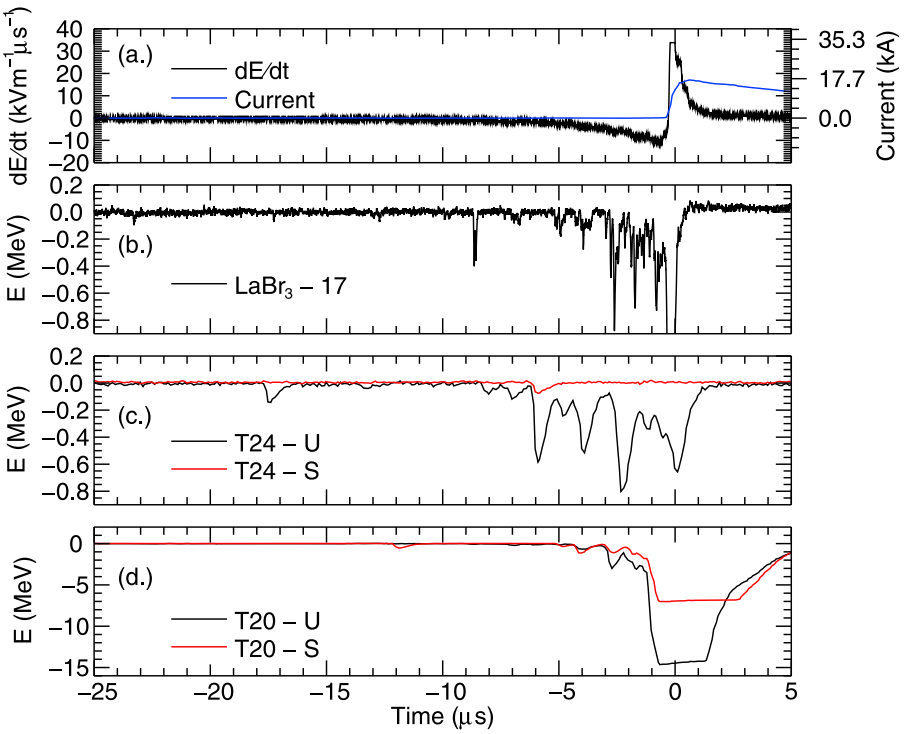

Figure 2. Waveforms of (a) electric field derivative, current (in blue) and (b) $LaBr_3$ and (c and d) NaI detectors for the "chaotic" leader UF 10-20. Shielded NaI PMTs are displayed (in red) in Figures 2c and 2d. The launch tower is located at station 20. Station 17 and station 24 are 39 m and 137 m away from the launch tower. Time t = 0 μs indicates the start of the return stroke.

exhibited irregular dE/dt signals prior to the return strokes. Specifically, the pulse shape, pulse width, and pulse separation are unique from more typical dart and dart-stepped leaders [*Hill et al.*, 2012].

[19] Figure 2 shows the complete waveform (from −25 μs to 5 μs after the onset of the return stroke) for one of these "chaotic" leaders (UF 10-20). Current, dE/dt, and the anode signal from four NaI and one $LaBr_3$ detector are also displayed. The unique characteristics (i.e., pulse shape and pulse separation) cannot be seen in the current and electric field derivatives for Figure 2, but on the microsecond timescale these characteristics are apparent.

[20] Each lightning leader is analyzed using the data from NaI and/or $LaBr_3$/PMT detectors. The $LaBr_3$/PMTs were used in creating the energy spectrum. Both shielded and unshielded NaI/PMTs were used to produce all other figures including the radial profile. Since NaI/PMTs have slow response times, due to the inherent slow light decay time constant, the output current limit on the PMT base, and the limited dynamic range of the Opticomm transceivers, pulses tend to pile-up and saturate. Only the deposited energy could be attained with the NaI/PMTs for measuring in the radial profile.

[21] In order to produce an accurate energy spectrum using data from the $LaBr_3$ detector, the detector response function found from a background X-ray pulse composed of a single photon was fitted to the measured data. Since the pulse shape changes with amplitude due to the slew-rate of the amplifier and the PMT's saturation, three different pulses, one with high signal amplitude, one with medium signal amplitude, and one with a low signal amplitude, were used. These single photon pulses were compiled from a time period when X-ray emission from lightning was not present. This allows the photon energies to be extracted from the anode waveforms. Once the background pulse fits the measured data, an amplitude can be extracted, which is then multiplied by a calibration factor to produce the corrected energy. By calibrating with five radioactive sources, it was found that the pulse height energy relation remains linear up to 1.3 MeV. No conclusions about the linearity can be made beyond this energy. Using this fact, the energies measured were calibrated with a Cs-137 (662 keV) radioactive source.

[22] In Figure 3, the overall best fit is shown in red. The blue curve is the detector response found from the measured data of a known single photon pulse. As seen in Figure 3, the blue curves, or photon pulses, were fit to the leader emission starting from the beginning of the emission and continuing to the return stroke. Each photon pulse was added to the previous pulse to produce the red curve (It should be noted that if multiple photons arrive in the detector at exactly the same time, each photon response could be several photons summed together).

[23] Pulse pile-up is also a concern when fitting pulses to the measured data. If the measured pulses arrive too close to each other, pile-up occurs, which will sum the deposited energy of the pulses together (see Figure 3). The actual pulses (in blue) are very close together, which results in an extended emission as shown in the measured data (in black). If the measured data were not fit using multiple single photon pulses, the photon energies would be significantly overestimated. If this is the case, the high energy tail of the energy

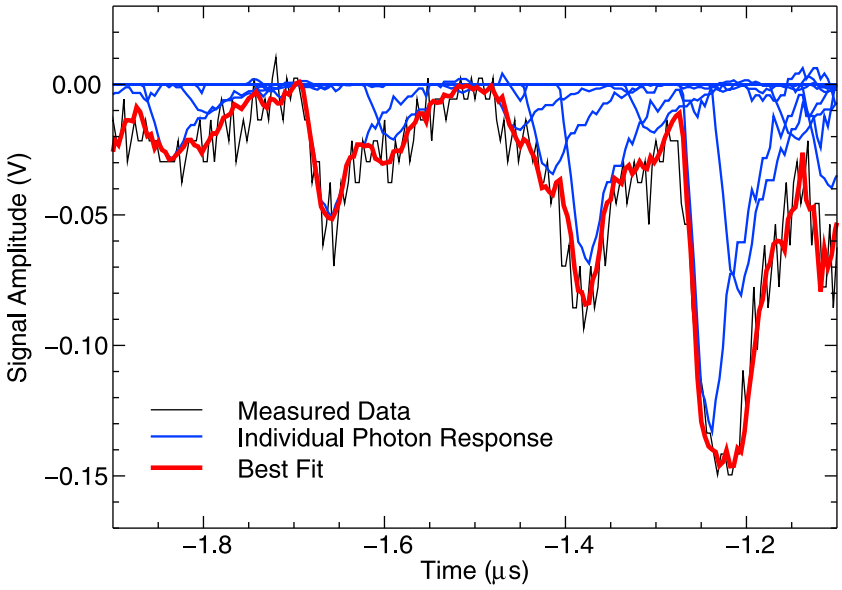

Figure 3. An expanded view of an X-ray waveform from UF 10-20 from −1.9 to −1.1 μs prior to the start of the first return stroke. The black line indicates the measured data and the blue line indicates the individual photon response. The red line, which is the sum of the individual pulses, closely matches the measured data. The slight fluctuations from the measured data are due to the fact that each blue curve is measured data of a known single photon pulse.

spectrum will be overestimated while the low energy part will be underestimated.

[24] MSE 10-01, a one-stroke negative cloud-to-ground flash, terminated on the ground in the southwest corner of the ICLRT site. The strike point location can be seen at the center of Figure 4. During this event, the time-of-arrival (TOA) network along with the MSE and TERA networks were all recording. Two high speed cameras, both Phantom V310 located at the office trailer and launch control, captured this flash. The camera at launch control and the office trailer were operated at 3.2 kfps (kilo-frames per second) and 4.2 kfps, respectively. The camera located at launch control captured a

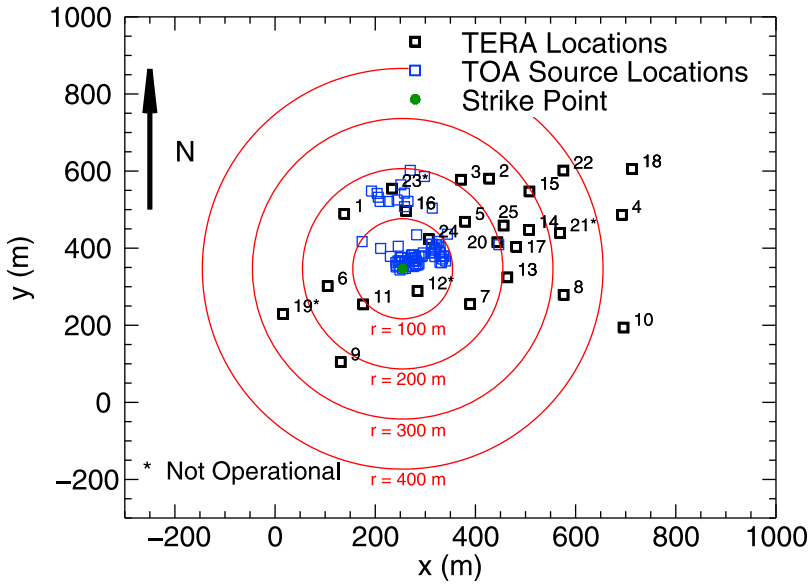

Figure 4. Locations of the TERA stations with the TOA source locations (in the x-y plane) from MSE 10-01 overlaid. Fourteen unshielded and 4 shielded detectors are operational on the site for the flash MSE 10-01. The dE/dt TOA source locations span about 250 m. The approximate strike point location is located in green. The origin of the Monte Carlo cylindrical volume source model is also the strike point. The model's cylindrical volume in this case was chosen to have a radius of 250 m, which completely encases the TOA source locations. Concentric red annuli indicate the radial distance from the strike point that is used in the model.

downward negative and upward connecting positive leader. The upward positive leader was positioned where the eventual strike point was located. In the frame of the return stroke, on the same camera, an upward propagating leader was seen to the south of the return stroke. Three main branches were seen in the frame before the return stroke. Within each main branch, several smaller branches can be seen. Of the three branches, the one farthest to the south was the branch that terminated to the ground.

[25] MSE 07-04 was a natural negative cloud-to-ground flash that terminated about 200-m west of the ICLRT site. The derivative electric field pulses were loosely separated by 100 to 200-m into two regions, which is similar to the stepped leader phase of other natural lightning strokes. Further details about MSE 07-04 are described in *Howard et al.* [2010].

[26] UF 10-20, data from which are shown in Figure 2, was a rocket-triggered negative cloud-to ground dart leader that produced four subsequent return strokes. The energetic radiation during the period prior to the first return stroke (the dart leader phase in this case) will be analyzed in this paper. Specifically, this "chaotic" dart leader exhibits unusual dE/dt measurements similar to "chaotic" leaders from *Wiedman* [1982], *Rakov and Uman* [1990], and *Hill et al.* [2012]. The return stroke following the "chaotic" dart leader produced a peak current of about 17 kA and the leader produced a continuous burst of X-rays, unlike the discrete bursts that are usually measured in other dart-stepped leaders.

4. Modeling

[27] Natural and triggered lightning produce runaway electrons and bremsstrahlung X-rays in strong electric fields as the electrons interact with air molecules [*Dwyer et al.*, 2005]. To model these mechanisms, detailed Monte Carlo simulations of runaway electron propagation of air were used. Specifically, the characteristics of the energetic electron source populations will be investigated. When using TERA, the effect of X-rays interacting with air become important because the array is spread over such a wide area.

[28] The simulation includes all interactions affecting energetic electrons and positrons, which involve energy losses through ionization and atomic excitation, Møller scattering for secondary electron production, and electron scattering [*Dwyer et al.*, 2003; *Dwyer*, 2004, 2007; *Dwyer and Smith*, 2005]. Photon (X-ray and gamma-ray) interactions including photoelectric absorption, coherent and Compton scattering, and pair production are also modeled. In addition, bremsstrahlung production of X-rays and gamma-rays from all secondary electrons and positrons and gamma-rays from positron annihilation are also simulated. Since we are modeling the interactions with particle detectors located at ground level, backscatter and absorption of X-rays with the soil are included. Effects from the instrument itself, including lead and aluminum, are also considered and corrected for within the Monte Carlo model.

[29] Since X-rays are strongly associated with stepping in natural lightning, the source is expected to be located near a strong electric field at the leader tip. In the modeling, the energetic electrons are located in this high field region and only move a short distance to produce X-rays. The spectrum of the energetic electrons is assumed to be initially of the form $dN_e/\mathrm{dK} \propto \exp(-\mathrm{K}/K_0)$ where K is the kinetic energy of the runaway electrons [*Lehtinen et al.*, 1999; *Dwyer*, 2004]. This assumption is motivated by the exponential energy spectrum with an e-folding kinetic energy, K_0, of 7.3 MeV produced during RREA multiplication. In this study, K_0 is allowed to vary and is chosen to best fit the data. With this energy spectrum, the runaway electrons are propagated through air where both the magnetic and electric fields are set to zero. The Earth's magnetic field has been demonstrated to have no significant impact on the simulation's results [*Dwyer and Smith*, 2005].

[30] The simulations are based on a model where a stepped leader radiates electromagnetic pulses followed by X-ray emission, both co-located in 3D coordinate space above the ground. Using the electric field derivatives, TOA source locations are measured and the position and velocity of the source is calculated [*Howard et al.*, 2010]. According to the dE/dt TOA source locations produced from MSE 10-01, the source propagated from about 290 m to about 17 m at an average speed of 4.22×10^5 m/s. MSE 07-04 and UF 10-20, had average speeds of 9.0×10^5 m/s and 2.55×10^7 m/s, respectively [*Howard et al.*, 2010]. This velocity is in agreement with other natural and rocket-triggered lightning velocities that have been previously measured. MSE 10-01 was modeled as an X-ray producer using two separate techniques: a line source technique and a volume source technique. The line source, proposed by *Saleh et al.* [2009] describes the X-ray source as a point source that moves in the vertically downward negative z-direction with the dE/dt sources. When integrated over all time, the X-ray source, therefore, forms a vertical line. This model is used primarily for on-site rocket-triggered lightning and natural lightning that terminated off-site. Similarly, the volume source model describes the X-ray source as a uniform disk that moves vertically downward when integrated over time, the X-ray source forms a cylinder with radius r, located over the ICLRT site. The volume source model can be used for natural lightning that terminates on the ICLRT site and contains a broad region of emission. Evidence from the literature [*Dwyer et al.*, 2005; *Rakov and Uman*, 2003; *Howard et al.*, 2010; *Schonland et al.*, 1938, 1956] suggest that different branches in a stepped leader might act as distributed point sources that can be simplified as a volume source. The strike point is chosen as the origin of the volume source model. The radius of the cylindrical volume can be varied depending on the natural lightning event. The origin for the line source model is considered to be the strike point of the event.

[31] Based on the results proposed by *Saleh et al.* [2009], an isotropic electron source was chosen for all three lightning events. Energetic electrons are injected uniformly into the downward-moving hemisphere of velocity space. As they propagate through air, they undergo elastic scattering with air atoms, which causes an angular diffusion of the electron's velocity vectors thus producing a more isotropic distribution. As the electrons propagate, they also emit bremsstrahlung X-ray photons. These photons have an approximate 1/E energy spectrum of the emitting electrons and are also emitted with an angular distribution with an angular width of about $1/\gamma$, where γ is the Lorentz factor of the electron. The source was modeled at 4 different initial characteristic energies: 300 keV, 1 MeV, 3 MeV, and 7 MeV.

[32] The energetic electrons are injected into the simulation at the source altitude (determined by the dE/dt TOA location

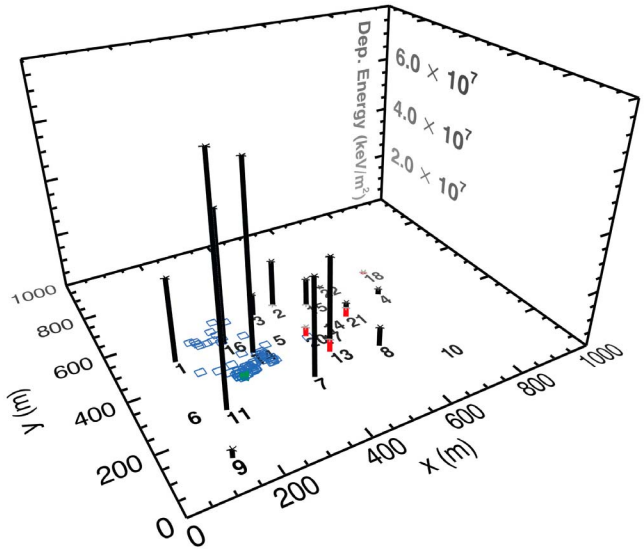

Figure 5. Deposited energy of each TERA station with the dE/dt TOA source locations projected on the x-y plane (blue) from MSE 10-01 overlaid. The black and red lines indicate deposited energy from the unshielded and shielded detectors, respectively. The green marker indicates the strike point location. The increasing x and y axes indicate an east and north heading, respectively.

estimates of the leader tip position) of the lightning event and propagated until it loses energy and stops. The model then propagates the photons until they are absorbed or drop below an energy of 30 keV, which is the approximate lower sensitivity limit that the PMTs can detect when placed inside the aluminum TERA boxes. A ground plane at (z = 0 m) is positioned to collect the X-ray emission from the simulation and the simulated data are divided into a set of concentric annuli positioned around the origin (strike point).

5. Results

5.1. Spatial and Energy Distributions

[33] Figures 5 and 6 show the measured deposited energy of each TERA station from MSE 10-01 and MSE 07-04. The vertical lines show the deposited energy from the unshielded (black) and shielded (red) detectors, respectively. 14 unshielded and 4 shielded detectors are operational on the site for the flash MSE 10-01. The blue squares indicate dE/dt TOA source locations projected on the x-y plane. The increasing x and y axes in both figures indicate an east and north heading, respectively. Figure 5 shows a broad region of deposited energy on the TERA detectors across the ICLRT site. As can be seen, the dE/dt TOA source locations are located close to the TERA detectors with the highest energies deposited. Figure 6 shows TOA source locations from a natural stepped leader that terminated to ground off-site – about 200 m. The TERA stations closest to the lightning display the highest energies deposited. The X-ray emission from both stepped leaders measured maximum deposited energies on the order of 10^7 keV/m^2.

[34] The radial distributions, luminosities, and energy spectra for two natural stepped leaders and one rocket-triggered "chaotic" dart leader are shown in Figures 7 through 13. It should be noted that stepped leaders precede first return strokes of natural lightning, two of which are analyzed in this report in detail, while rocket-triggered lightning have return strokes preceded by dart, dart-stepped, and "chaotic" dart leaders. Figure 7 shows the radial distribution for MSE 10-01 using both a line and a volume source model. Any detectors that displayed saturation are shown as upward arrows. Also, the energy deposited on the unshielded and shielded detectors have been radially binned and plotted at the midpoint of each annulus for clarity. For MSE 10-01, saturation occurred in detectors with a radial distance less than 250 m from the strike point. Monte Carlo simulations are used to predict the number of photons detected because they are not known in the measurements, which allows the Poisson errors to be found. Specifically, these simulations can estimate the average energy per photon, which is then used in combination with the measured deposited energies to calculate the number of photons detected. The number of photons detected is then used to determine the approximate RMS variations that should occur in the deposited energies similar to *Saleh et al.* [2009].

[35] Figure 7a displays the best fit of all the volume source models using the chi-square goodness-of-fit computation. The distribution seems to flatten out from about 0 m to 250 m and then quickly falls off thereafter. It should be noted that only 4 shielded detectors (1 located between 0–100 m and 3 located between 200–300 m) were operational during the flash MSE 10-01. Since TOA source locations spanned radially about 250 m (see Figure 4), the cylindrical volume source model in this case was chosen to have a radius of 250 m so that the model's cylindrical volume completely encases the TOA source locations. The 1 MeV model fits the

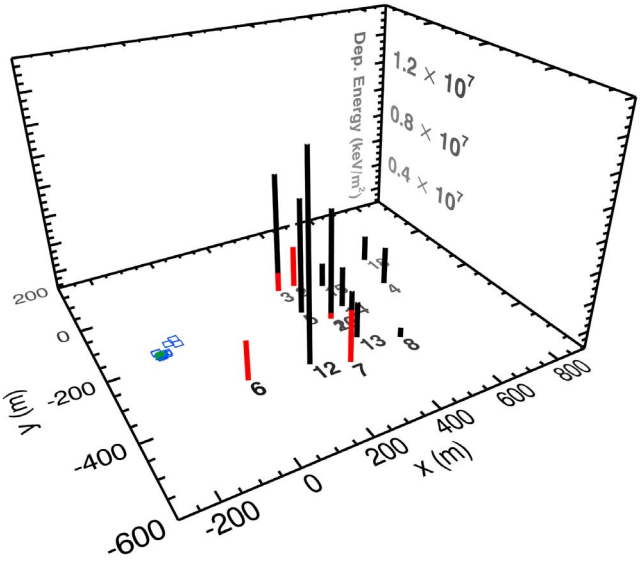

Figure 6. Deposited energy of each TERA station with the dE/dt TOA source locations projected on the x-y plane (blue) from MSE 07-04 overlaid. The black and red lines indicate deposited energy from the unshielded and shielded detectors, respectively. The green marker indicates the strike point location. The increasing x and y axes indicate an east and north heading, respectively. This stepped leader occurred about 200 m off-site.

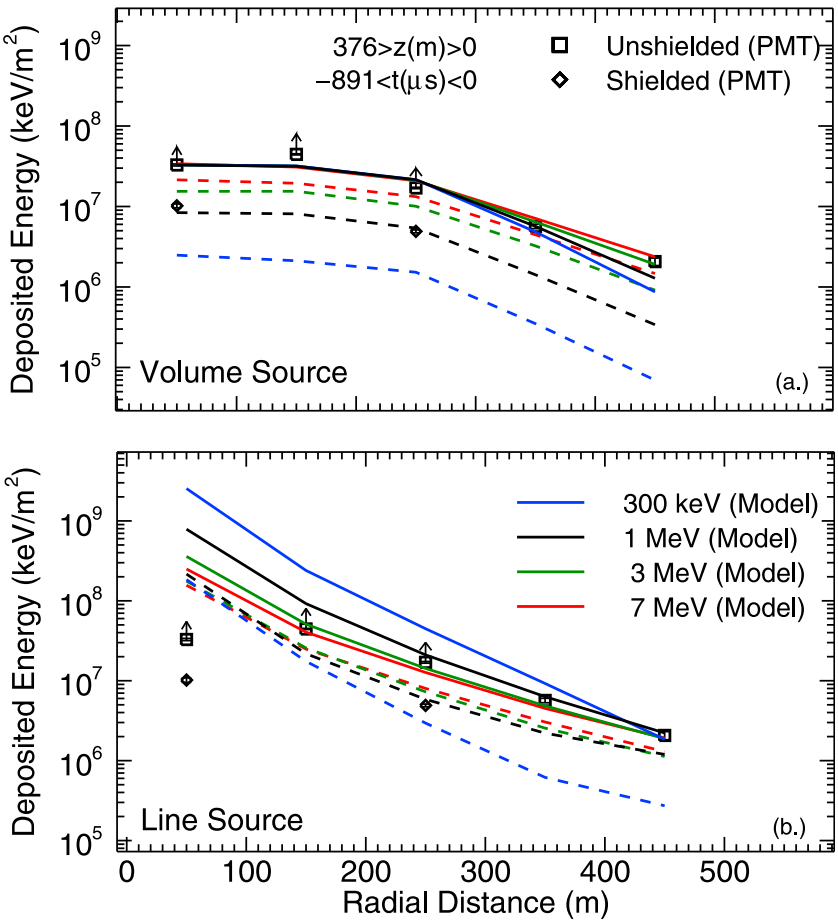

Figure 7. Deposited energy versus radial distance for MSE 10-01 along with Monte Carlo (a) volume and (b) line source model results for four isotropic energetic electron sources. The square and diamonds indicate the energy deposited on unshielded and shielded detectors that have been radially binned (each bin equaling 100 m) and plotted at the midpoint of each annulus for clarity. Solid and dashed lines also display the modeled deposited energy from the unshielded and shielded detectors, respectively.

data best in this case, although large uncertainties occur since this leader shows saturation radially outward to 250 m. Figure 7b shows the fits of the line source model normalized to the furthest right point located at 450 m. This model produced a distribution that falls off quickly as the radial distance is increased and does not agree well with the measured data. However, if the measured data are heavily saturated, the first three radial binned points could be underestimated. As a result, these observations cannot completely rule out the line source model. If this is the case, these data points would be shifted upward, potentially agreeing with the 1 MeV or 300 keV modeled electron source spectrum. At any rate, both the line and volume source models indicate that the electron source has a characteristic energy between 300 keV to 1 MeV.

[36] Figure 8 shows the radial distributions for a set of altitude regions, which correspond to three time intervals of about 250 μs periods prior to the return stroke. In other words, Figure 8 ranges from -237 μs to 0 μs, -474 μs to -237 μs, and -891 μs to -474 μs prior to the start of the return stroke, respectively. All three plots use 300 keV and 1 MeV characteristic energy (with volume source) models to fit the data. In particular, Figure 8a, the 1 MeV source model fits the data for from z = 0 m to 100 m. In Figure 8b, with source altitudes ranging from z = 100 m to 200 m, the 1 MeV model produces results that overestimate the deposited energy compared with the data, but the 300 keV source model is a better fit to the data. Figure 8c overestimates the 300 keV electron source model (out of the 1 MeV and 300 keV models) and appears to contain an electron source energy of <300 keV. Unfortunately, only one radially binned point remains on the shielded detectors for the altitude region in Figure 8c. In Figures 8b and 8c, saturation does not occur, allowing the line and volume source models to be compared. In both cases the volume source model gives a better fit of these altitudes. Figure 8a is shown using the volume source model, but could be described also using the line source model as well, since it is saturated out to 250 m. In either model, the 1 MeV characteristic energy spectrum seems to fit best for source location altitudes between 0 m to 100 m. As a result, the characteristic energy of the source appears to increase as it approaches the ground.

[37] Using the best fit models at each altitude range, the source electron luminosity was found as a function of height above the ground (see Figure 9). Above altitudes of 291 m, the location of the source altitude is not known. Thus, it is

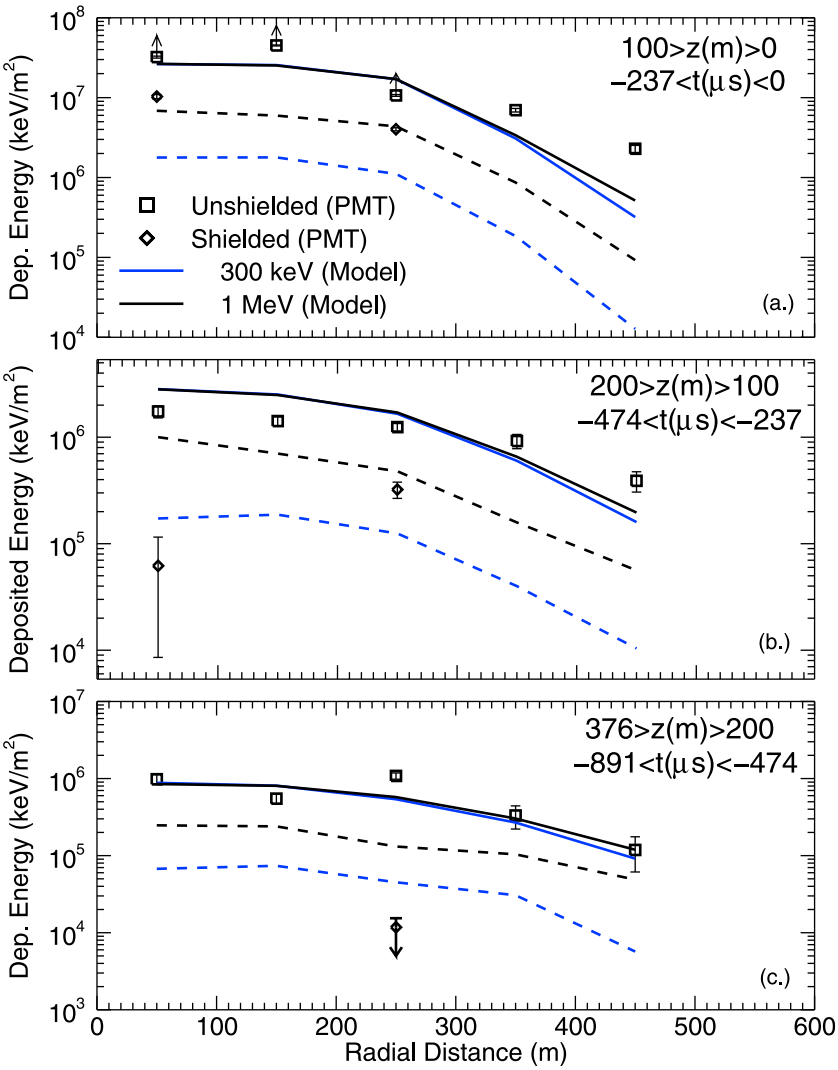

Figure 8. Deposited energy versus radial distance for MSE 10-01 along with Monte Carlo volume source model results for two isotropic energetic electron sources for varying altitudes. The square and diamonds indicate the energy deposited on unshielded and shielded detectors. Solid and dashed lines also indicate the modeled deposited energy from the unshielded and shielded detectors, respectively. (a) For altitudes from 0 to 100 m and −237 μs prior to the return stroke at t = 0. (b) For altitudes ranging from 100 m to 200 m and −237 to −474 μs before the return stroke. (c) For altitudes ranging from 200 m to 376 m and −474 to −891 μs before the return stroke.

assumed that the stepped leader above 291 m has the same velocity as the stepped leader below 291 m. The average luminosity for the electrons throughout the entire channel reached about 10^{14} electrons/s using the volume source model and about 10^{15} electrons/s for the line source model. The maximum X-ray luminosity, in the 0–100 m range, reached about 10^{13} s^{-1} for a 1 MeV electron source.

[38] Since both the volume and line source Monte Carlo model could fit the radial distributions from MSE 10-01, both models were used to determine the energy spectra. Figure 10 shows data from one $LaBr_3$/PMT detector, which extends up to energies of about 2 MeV, with model fits using the volume and line source models. The electron source can be determined accurately for energies up to 1.3 MeV due to the fact that calibration sources can only show linearity up to that energy as mentioned previously. For this leader, the lower sensitivity energy limit was determined to be about 91 keV. The 1 MeV modeled source spectrum was fit to the data using the least squares method. The other energies were then normalized to the 1 MeV spectrum to display the differences at higher energies. The error bars less than 1 MeV, indicate the statistical errors associated with Poisson fluctuations. The upper limits are the result of not detecting any X-rays on the ground at these higher energies with a 1σ confidence. The 3 MeV and 7 MeV electron source spectra significantly overestimates the measured energy spectrum at higher energies for this event. Regardless of source model chosen, both the 1 MeV and 300 keV agree within the uncertainties of the data.

[39] Figure 11 shows Monte Carlo models for MSE 07-04. Due to the fact that this stepped leader terminated off-site, the radial distributions extend to greater than 200 m. No TERA

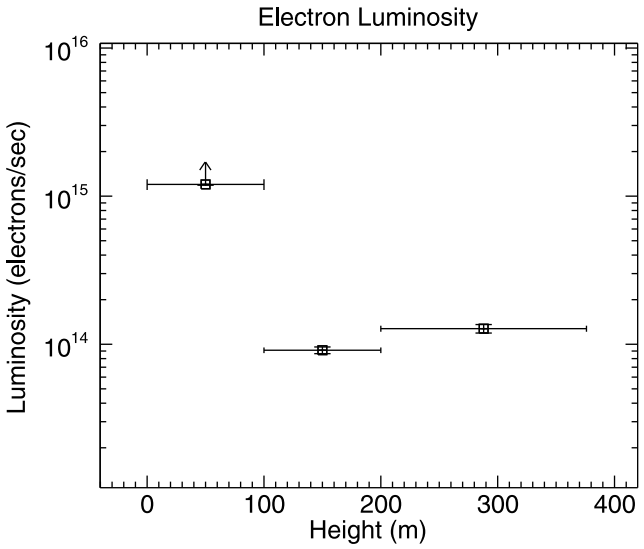

Figure 9. The electron luminosity emitted by the stepped leader from MSE 10-01. The upper arrow indicates the limit on the luminosity due to the saturation of the detectors. For altitudes between 0–100 m and 100–300 m, a 300 keV and 1 MeV modeled electron source was used to determine the electron luminosities, respectively.

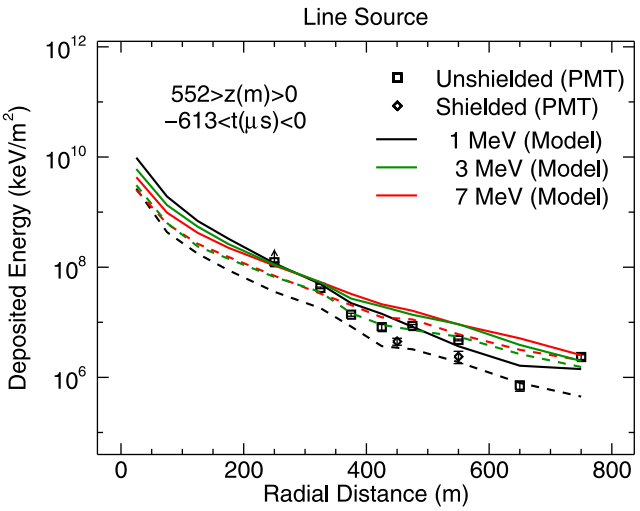

Figure 11. Deposited energy versus radial distance for MSE 07-04 along with Monte Carlo line source model results for three isotropic energetic electron sources. The square and diamonds indicate the energy deposited on unshielded and shielded detectors. Solid and dashed lines also indicate the modeled deposited energy from the unshielded and shielded detectors, respectively.

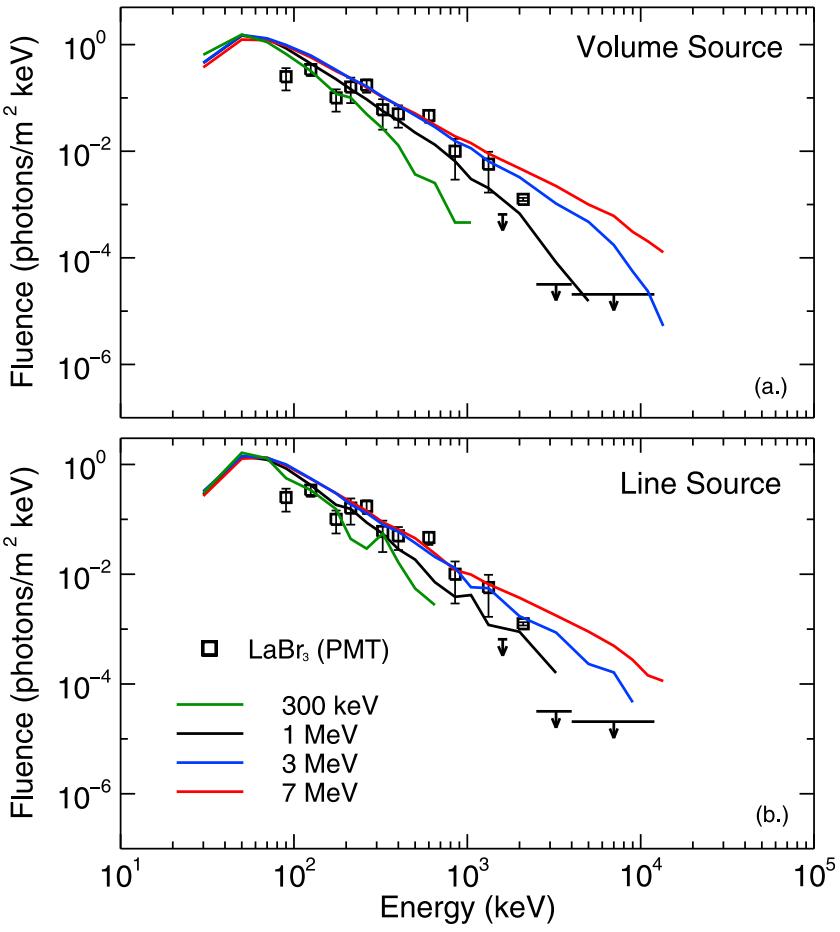

Figure 10. Energy spectra for MSE 10-01 along with Monte Carlo simulations for four different electron energy sources. The upper limits indicate no $LaBr_3$/PMT measurements on the ground at higher energies. (a) Volume Source Model. (b) Line Source Model.

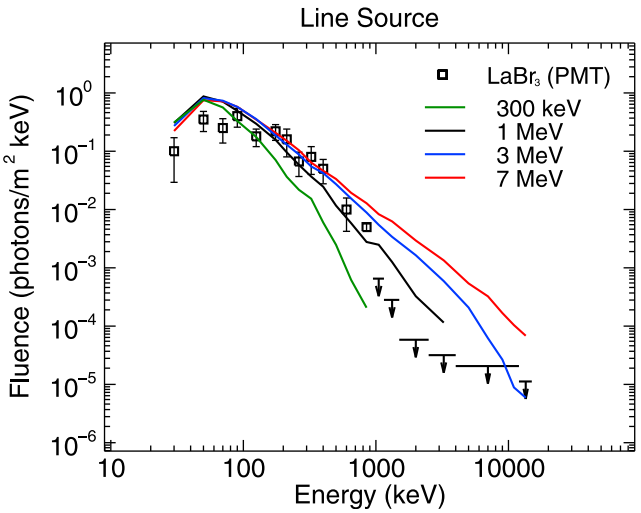

Figure 12. Energy spectra for UF 10-20 (chaotic dart leader) along with Monte Carlo simulations for four different electron energy sources. The upper limits indicate no measurements on the ground at higher energies.

stations were located any closer to this event. Unlike the radial distribution from MSE 10-01, MSE 07-04 exhibits a narrow emission over a small region to the west of the TERA stations. MSE 07-04 also can be seen at least up to 750 m, extending to the furthest detectors on the ICLRT site, which means that X-rays can be detected up to at least 800 m radially away from the source. Even with its great distance, saturation still occurred over 200 m from the source. In this event, Monte Carlo simulations were used to simulate a line source (i.e., a source that only propagates in the negative z-direction), since the emission appears to be limited to a small radial area. These simulations fit the general shape of the radial distribution, but do not definitively show the characteristic energy of the electron source.

[40] Figure 12 shows the energy spectrum for one leader from triggered lightning event UF 10-20 along with the line source simulation results, which contain energies ranging from 30 keV up to about 1 MeV. Since this event was a rocket-triggered leader, a line source was chosen. Similar to Figure 10, this energy spectrum also displays four different modeled energy spectra with various characteristic energy sources and was normalized similarly to the last two figures shown in this paper. Again, the 3 MeV and 7 MeV electron source spectra overestimate the $LaBr_3$ data. Both spectra, MSE 10-01 and UF 10-20, exhibit the same general spectral shape. Figure 13 shows the spatial energy distribution for UF 10-20, which shows a characteristic energy source somewhere between 300 keV and 1 MeV. If pulse pile-up was present the 3 MeV and 7 MeV spectrum would still not agree with measured data, since the presence of pile-up would mean that the true spectrum is softer. The luminosity was also calculated in a similar manner to MSE 10-01. The average luminosity was calculated to be on the order of about $\sim 10^{17}$ electrons/s at ground level.

5.2. Other Characteristics of Leaders From 2009–10

[41] Out of 12 different flashes, 103 lightning peak current pulses, some of which were identified as return strokes and some as M-components, were analyzed in Figures 14 and 15. All data were from 2009–10 and involved only rocket-triggered lightning. "Chaotic" type, dart and dart-stepped leaders were analyzed to find the electron luminosity, total energy, and energetic electrons per meter (i.e., the number of electrons per meter of downward propagation) versus each return stroke peak current following the leader using their spatial and energy distributions.

5.2.1. Luminosity and Total Energy

[42] Return strokes can be categorized as peak current pulses from lightning, having fast (<5 μs) risetimes whereas M-components pulses are current pulses with longer (>10 μs) risetimes. While the waveshape division is arbitrary, M-components are generally considered to occur while continuous current is flowing. M-components are often observed in current measurements to be symmetric pulses of an amplitude between 100–200 A with tens to hundreds of μs risetime. Occasionally, M-components have been measured in the kiloampere range, similar of that to a return stroke. The risetime is defined to be the required time for the current signal to transition from 10% of its lowest value to 90% of the peak current. Specifically, natural first return stroke peak currents have risetimes of 3–5 μs (for 10–90% current rate of rise). Subsequent return stroke peak currents typically have risetimes of 0.3–0.6 μs [*Rakov and Uman*, 2003]. In the 103 lightning peak current pulses, 71 M-components (peak current pulses during the continuing current as seen on Figure 14) and 28 return strokes were observed. Out of the 103 lightning peak current pulses, no X-rays in the time prior were visible in association with 75 (see Figure 14). Out of these 75 peak current pulses, 71 were M-components, and 4 appear to be return strokes that did not exhibit X-rays in their leader phase. Figure 14a shows the peak current pulse

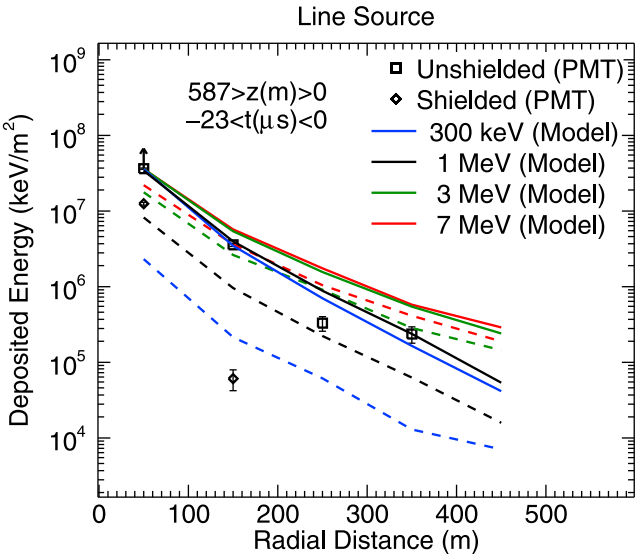

Figure 13. Deposited energy versus radial distance for UF 10-20 along with Monte Carlo line source model results for four isotropic energetic electron sources. The square and diamonds indicate the energy deposited on unshielded and shielded detectors. Solid and dashed lines also indicate the modeled deposited energy from the unshielded and shielded detectors.

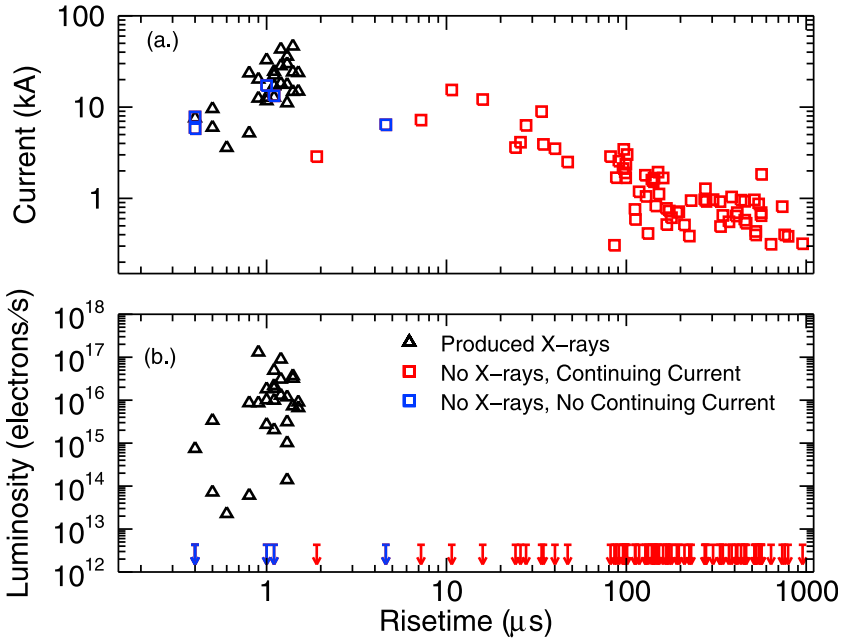

Figure 14. (a) The peak current pulse risetime versus the peak current pulse amplitude. (b) The electron luminosity of the last 15 microseconds prior to the start of the peak current pulse versus the peak current pulse risetime. In the 103 lightning peak current pulses, 71 M-components (red) and 28 return strokes (black) were observed. No X-rays in the time prior were visible in association with 75 (blue and red). Out of these 75 peak current pulses, 71 are M-components, and 4 are return strokes (blue) that did not exhibit X-rays in their leader phase. The non-producing X-ray cases are shown as upper limits corresponding to 4×10^{12} electrons/s, the upper limit for non-detection. Out of the 12 flashes investigated in this report, 100% of the times preceding M-components and 99% of time preceding peak current pulses with risetimes greater than 2 μs did not produce X-rays.

amplitude versus its risetime. Figure 14b shows the peak current pulse risetime versus the electron luminosity. The non-producing X-ray cases are plotted as upper limits of 4×10^{12} electrons/s, which is the upper limit for non-detection. Out of the 12 flashes investigated in this report, 100% of the times preceding M-components and 99% of time preceding peak current pulses with risetimes greater than 2 μs did not produce X-rays.

[43] By selecting just the leaders of the return strokes in Figure 14, Figure 15a shows the electron luminosity in electrons per second versus the return stroke peak current for the last 15 μs prior the start of the return stroke. For the return stroke currents ranging from 3 kA to 10 kA, a sharp increase in electron luminosity can be seen. For currents greater than 10 kA, the electron luminosity seems to plateau at values no greater than about 10^{17} electrons/s.

[44] Monte Carlo simulations were fitted to the spatial energy distributions to calculate the electron luminosity. For each leader (exception of one chaotic and one dart-stepped leader), saturation of the detectors occurred for radial distances less than 100 m. Saturation occurred for a radial distance less than 300 m for the other two leaders. In all cases, a Monte Carlo model was fitted to the radial energy distributions. The saturated tubes were included in these fits since the electron luminosity would only decrease if the saturated tubes were removed. If the detectors were saturated further than 300 m, the electron luminosity could be much greater than what the fit is producing. As a result, lower limits (shown in Figure 15 as upper arrows) are shown in this case. Previously in the paper, it was concluded that the energy at the source of natural and rocket-triggered leaders is between 300 keV and 1 MeV. Error bars in Figure 15 account for the uncertainty in electron luminosity for source energies ranging between these values.

[45] Figure 15b shows the total energy that was deposited on the ICLRT site during the leader phase versus return stroke peak current. Once again, the lower arrows account for no measurements at ground level, while the upper arrows account for saturation in the detectors. Similar to Figure 15a, a sharp increase can be seen in the total energy from 3 kA to 10 kA and then the shape of the measurements plateaus for events with return stroke currents greater than 10 kA. Figure 15b is completely independent from the model, which is dissimilar from Figures 15a and 15c. Since there is no dependence on the source for this figure, the total energy could be much greater for the saturated tubes especially for radially distances less than 100 m.

[46] Figure 15c shows the energetic electrons per meter of downward propagation versus return stroke current for three types of lightning leaders. The arrow bars and limits were found in a similar fashion as in Figure 15a. This figure illustrates that dart-stepped leaders emit more electrons per meter of downward propagation than both dart and chaotic type leaders. The dart, dart-stepped, and "chaotic" dart leaders all produce comparable amounts of electron luminosity over the entire leader channel, but since the dart-stepped leader is an order-of-magnitude slower, it produces more electrons per meter of downward propagation.

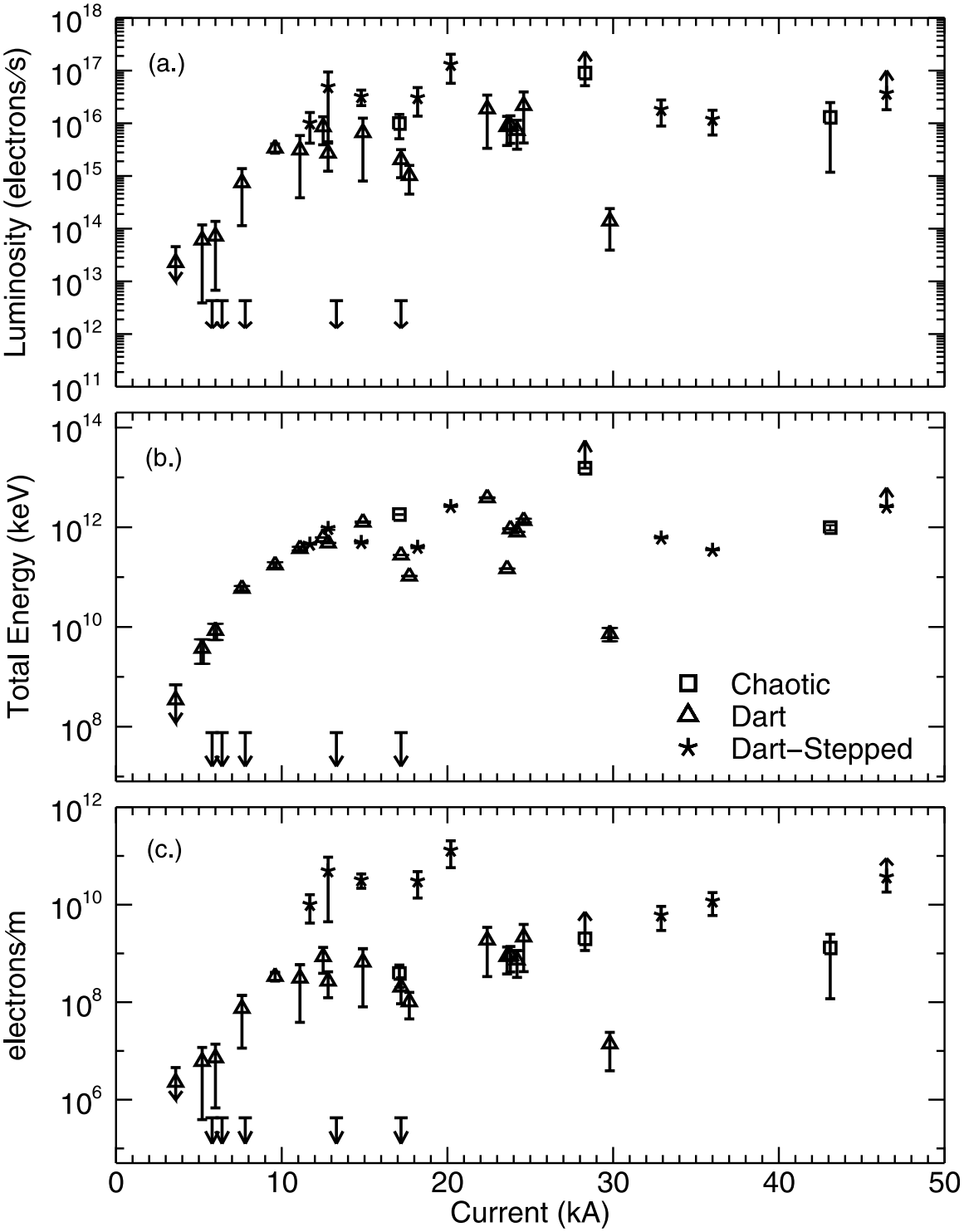

Figure 15. (a) The electron luminosity versus the return stroke peak current. (b) The total energy versus the return stroke peak current. (c) The amount of energetic electrons per meter of downward propagation versus the return stroke peak current.

5.2.2. Radiation Dose

[47] The radiation dose near the ground was estimated for each of the 28 leaders that emitted X-rays. The equation for effective dose is $E = h_{re}\Phi_{re}$ where h_{re} is the conversion factor that converts fluence to dose equivalent in the AP direction and Φ_{re} is the runaway fluence [*Katagiri et al.*, 2000; *Pelliccioni*, 2000; *Dwyer et al.*, 2010]. At 1 MeV, h_{re} is 7×10^{-12} *Svcm*^{2} and for 300 keV 1×10^{-15} *Svcm*^{2}. Since the electron luminosity was calculated for the last 15 μs before the start of the return stroke, the leaders emitted 10^8 to 10^{12} energetic electrons for all X-ray emitting leaders that were investigated here. The effective dose is found to be no

more than 10^{-4} Sv for an electron beam of 1 m. For electrons beams that are larger, the effective dose decreases. Given the fact that 10^{-3} Sv is the yearly dose that a person receives, this study has found that from each of the 28 leaders analyzed, the X-rays from a direct strike would not be harmful.

6. Discussion

[48] By comparing the Monte Carlo simulations to the energies deposited from both natural stepped leader events, we can ascertain that the X-ray emission is consistent with bremsstrahlung emission of the form $dN_e/\mathrm{dK} \propto \exp(-\mathrm{K}/K_0)$ where K_0 ranges between 300 keV to 1 MeV and the electron source has a characteristic energy of less than $K_0 = 3$ MeV. However, no conclusions can be made as to the exact spectral shape of the emission. Only an approximate energy scale can be determined. Additionally, the runaway electron intensity increases with a decrease in altitude as shown in Figure 8 for MSE 10-01. This is in agreement with *Dwyer et al.* [2004, 2005], who also noticed an increased intensity as the leader propagated toward the ground.

[49] Both stepped and dart leaders in this report exhibit electron characteristic energies less than 3 MeV. This differs from the RREA mechanism since RREA requires the average energy of electrons to be 7.3 MeV [*Dwyer*, 2004], which is inconsistent with the average energy results from the leaders analyzed here. For both cases, the stepped leader X-ray energy extends up to 1–2 MeV, which is higher than the 250 keV reported in *Dwyer* [2004]. The difference in energies could either reflect the variation in the energy spectrum from lightning or it could be explained by the fact that *Dwyer* [2004] assumed a downward beamed electron source whereas this report assumes an isotropic source, similar to *Saleh et al.* [2009]. As in other reports [*Saleh et al.*, 2009; *Dwyer*, 2004; *Moss et al.*, 2006], this report also supports the hypothesis by *Dwyer* [2004] that cold runaway breakdown is occurring [*Gurevich*, 1961]. This mechanism requires very strong electric fields, above 30 MV/m, to be nearby the leader or streamer tip [*D'Angelo*, 1987], accounting for the low range of characteristic energies since, unlike RREA, the runaway electrons may only gain modest energies in the electric field.

[50] The average electron luminosity of stepped leader emission reported here is about 1 to 2 orders-of-magnitude lower than that of the average luminosity of the one intense dart-stepped leader reported in *Saleh et al.* [2009], but the electron luminosity near the ground is in agreement with *Saleh et al.* [2009]. Previous unpublished observations at the ICLRT show that stepped leaders tend to be the brightest X-ray emitters of all types of leaders, but this report shows that the average luminosity seems to fall in the same range as the other types of leaders. One explanation for this discrepancy is that the source of emission could be much broader (i.e., many branches of X-rays emission), which could cause it to appear much brighter. No stepped leaders were plotted in Figure 15, since peak current measurements were unavailable. However if the stepped leaders in this report were plotted on Figure 15a, their average electron luminosities would fall in the same range as the other types of leaders. Furthermore, if the stepped leader cases were plotted on Figure 15c, they would show that the stepped leaders emit the highest electrons per meter, since stepped leaders have a lower propagation speed typically 2×10^5 ms^{-1}.

[51] The electron luminosity of lightning leaders appears to reach an upper limit for return stroke peak currents of 10 kA and greater. Electron luminosity does increase with increasing return stroke current for currents below about 10 kA, but reach a plateau thereafter. In other words, a high return stroke peak current following a leader does not imply a high electron luminosity for the leaders investigated in this paper. These measurements become important when modeling TGFs because the seed production rate is a fundamental input parameter in many TGF simulations. Current TGF models use theoretical electron luminosity values that range from 10^{18} electrons/s to 10^{19} electrons/s [*Moss et al.*, 2006; *Gurevich et al.*, 2007], which are larger than our typical measured values.

[52] Out of 103 lightning peak current pulses, 75 did not emit X-rays in the times prior to their lightning peak current pulse. Interestingly, 71 of these no X-ray emitting cases were pulses occurring during continuing current flow and exhibited a risetime greater than 2 μs. With almost 100% confidence, we conclude that no X-rays will be seen in the time preceding M-components with risetimes greater than 2 μs.

[53] **Acknowledgments.** We would like to thank those at Florida Tech and the University of Florida who assisted in the operation and maintenance of TERA. This work was supported in part by NSF grant ATM 0607885, NASA grant NNX09AJ07H, and DARPA grants HR0011-08-1-0088 and HR0011-1-10-1-0061.

References

D'Angelo, N. (1987), On X-rays from thunderclouds, *Ann. Geophys., Ser. B*, *5*, 119–122.

Dwyer, J. R. (2004), Implications of X-ray emission from lightning, *Geophys. Res. Lett.*, *31*, L12102, doi:10.1029/2004GL019795.

Dwyer, J. R. (2007), Relativistic breakdown in planetary atmospheres, *Phys. Plasmas*, *14*, 042901, doi:10.1063/1.2709652.

Dwyer, J. R. (2009), Energetic radiation and lightning, in *Lightning: Principles, Instruments, and Applications*, edited by H. D. Betz et al., pp. 331–346, Springer, Dordrecht, Netherlands, doi:10.1007/978-1-4020-9079-0.

Dwyer, J. R., and D. M. Smith (2005), A comparison between Monte Carlo simulations of runaway breakdown and terrestrial gamma-ray flash observations, *Geophys. Res. Lett.*, *32*, L22804, doi:10.1029/2005GL023848.

Dwyer, J. R., et al. (2003), Energetic radiation produced during rocket-triggered lightning, *Science*, *299*, 694–697.

Dwyer J. R., et al. (2004), Measurements of X-ray emission from rocket-triggered lightning, *Geophys. Res. Lett.*, *31*, L05118, doi:10.1029/2003GL018770.

Dwyer, J. R., et al. (2005), X-ray bursts associated with leader steps in cloud-to-ground lightning, *Geophys. Res. Lett.*, *32*, L01803, doi:10.1029/2004GL021782.

Dwyer, J. R., D. M. Smith, M. A. Uman, Z. Saleh, B. Grefenstette, B. Hazelton, and H. K. Rassoul (2010), Estimation of the fluence of high-energy electron bursts produced by thunderclouds and the resulting radiation doses received in aircraft, *J. Geophys. Res.*, *115*, D09206, doi:10.1029/2009JD012039.

Dwyer, J. R., D. M. Smith, S. A. Cummer (2012), High-energy atmospheric physics: Terrestrial gamma-ray flashes and related phenomena, *Space Sci. Rev.*, doi:10.1007/s11214-012-9894-0, in press.

Eack, K. B., W. H. Beasley, W. D. Rust, T. C. Marshall, and M. Stolzenburg (1996a), X-ray pulses observed above a mesoscale convection system, *Geophys. Res. Lett.*, *23*, 2915–2918.

Eack, K. B., W. H. Beasley, W. D. Rust, T. C. Marshall, and M. Stolzenburg (1996b), Initial results from simultaneous observations of X-rays and electric fields in a thunderstorm, *J. Geophys. Res.*, *101*, 29,637–29,640.

Gurevich, A. V. (1961), On the theory of runaway electrons, *Sov. Phys. JETP, Engl. Transl.*, *12*(5), 904–912.

Gurevich, A. V., and K. P. Zybin (2001), Runaway breakdown and electric discharges in thunderstorms, *Phys. Usp.*, *44*, 1119, doi:10.1070/PU2001v044n11ABEH000939.

Gurevich, A. V., G. M. Milikh, and R. A. Roussel-Dupré (1992), Runaway electron mechanism of air breakdown and preconditioning during a thunderstorm, *Phys. Lett. A*, *165*, 463–468.

Gurevich, A. V., K. P. Zybin, and Y. V. Medvedev (2007), Runaway breakdown in strong electric field as a source of terrestrial gamma flashes and gamma bursts in lightning leader steps, *Phys. Lett. A*, *361*(1–2), 119–125, doi:10.1016/j.physleta.2006.05.063.

Hill, J. D., M. A. Uman, D. M. Jordan, J. R. Dwyer, and H. K. Rassoul (2012), "Chaotic" dart leaders in triggered lightning: Electric fields, X-rays, and source locations, *J. Geophys. Res.*, *117*, D03118, doi:10.1029/2011JD016737.

Howard, J., M. A. Uman, C. Biagi, D. Hill, J. Jerauld, V. A. Rakov, J. R. Dwyer, Z. H. Saleh, and H. K. Rassoul (2010), RF and X-ray source locations during the lightning attachment process, *J. Geophys. Res.*, *115*, D06204, doi:10.1029/2009JD012055.

Katagiri, M., M. Hikoji, M. Kitaichi, S. Sawamura, and Y. Aoki (2000), Effective doses and organ doses per unit fluence calculated for monoenergetic 0.1 MeV to 100 MeV electrons by the MIRD-5 phantom, *Radiat. Prot. Dosim.*, *90*, 393–401.

Lehtinen, N. G., T. F. Bell, and U. S. Inan (1999), Monte Carlo simulation of runaway MeV electron breakdown with application to red sprites and terrestrial gamma ray flashes *J. Geophys. Res.*, *104*, 24,699–24,712, doi:10.1029/1999JA900335.

McCarthy, M. P., and G. K. Parks (1985), Further observations of X-rays inside thunderstorms, *Geophys. Res. Lett.*, *12*, 393–396.

McCarthy, M. P., and G. K. Parks (1992), On the modulation of X-ray fluxes in thunderstorms, *J. Geophys. Res.*, *97*(D5), 5857–5864, doi:10.1029/91JD03160.

Moore, C. B., K. B. Eack, G. D. Aulich, and W. Rison (2001), Energetic radiation associated with lightning stepped-leaders, *Geophys. Res. Lett.*, *28*, 2141–2144.

Moss, G. D., V. P. Pasko, N. Liu, and G. Veronis (2006), Monte Carlo model for analysis of thermal runaway electrons in streamer tips in transient luminous events and streamer zones of lightning leaders, *J. Geophys. Res.*, *111*, A02307, doi:10.1029/2005JA011350.

Pelliccioni, M. (2000), Overview of fluence-to-effective dose and fluence to ambient dose equivalent conversion coefficients for high energy radiation calculated using FLUKA code, *Radiat. Prot. Dosim.*, *88*, 279–297.

Rakov, V. A., and M. A. Uman (1990), Waveforms of first and subsequent leaders in negative lightning flashes, *J. Geophys. Res.*, *95*, 16,561–16,577.

Rakov, V. A., and M. A. Uman (2003), *Lightning Physics and Effects*, Cambridge Univ. Press, Cambridge, U. K.

Saleh, Z., J. Dwyer, J. Howard, M. Uman, M. Bakhtiari, D. Concha, M. Stapleton, D. Hill, C. Biagi, and H. Rassoul (2009), Properties of the X-ray emission from rocket-triggered lightning as measured by the Thunderstorm Energetic Radiation Array (TERA), *J. Geophys. Res.*, *114*, D17210, doi:10.1029/2008JD011618.

Schonland, B. F. J. (1938), Progressive lightning, part 4: The discharge mechanisms, *Proc. R. Soc. A*, *164*, 132–150.

Schonland, B. F. J. (1956), The lightning discharge, in *Handbook of Physics*, vol. 22, pp. 576–628, Springer, Berlin.

Suszcynsky, D. M., R. Roussel-Dupré, and G. Shaw (1996), Ground-based search for X-rays generated by thunderstorms and lightning, *J. Geophys. Res.*, *101*, 23,505–23,516.

Wiedman, C. D. (1982), The submicrosecond structure of lightning radiation fields, PhD dissertation, Univ. of Ariz., Tucson.

Wilson, C. T. R. (1925), The acceleration of beta-particles in strong electric fields such as those of thunder-clouds, *Proc. Cambridge Philos. Soc.*, *22*, 534–538.